

Article

Experimental and One-Dimensional Mathematical Modeling of Different Operating Parameters in Direct Formic Acid Fuel Cells

Shingjiang Jessie Lue ^{1,2,3,*} , Nai-Yuan Liu ¹, Selvaraj Rajesh Kumar ¹, Kevin Chi-Yang Tseng ¹, Bo-Yan Wang ¹ and Chieh-Hsin Leung ¹

¹ Department of Chemical and Materials Engineering and Green Technology Research Center, Chang Gung University, Guishan District, Taoyuan City 333, Taiwan; nyliu11235@gmail.com (N.-Y.L.); rajeshkumarnst@gmail.com (S.R.K.); kevin_cyt@hotmail.com (K.C.-Y.T.); sebsilica@gmail.com (B.-Y.W.); hsin_1015@yahoo.com.tw (C.-H.L.)

² Department of Radiation Oncology, Chang Gung Memorial Hospital, Guishan District, Taoyuan City 333, Taiwan

³ Department of Safety, Health and Environment Engineering, Ming-Chi University of Technology, Taishan, New Taipei City 243, Taiwan

* Correspondence: jessie@mail.cgu.edu.tw; Tel.: +886-3-211-8800 (ext. 5489); Fax: +886-3-211-8700

Received: 15 October 2017; Accepted: 23 November 2017; Published: 27 November 2017

Abstract: The purpose of this work is to develop a one-dimensional mathematical model for predicting the cell performance of a direct formic acid fuel cell and compare this with experimental results. The predicted model can be applied to direct formic acid fuel cells operated with different formic acid concentrations, temperatures, and with various electrolytes. Tafel kinetics at the electrodes, thermodynamic equations for formic acid solutions, and the mass-transport parameters of the reactants are used to predict the effective diffusion coefficients of the reactants (oxygen and formic acid) in the porous gas diffusion layers and the associated limiting current densities to ensure the accuracy of the model. This model allows us to estimate fuel cell polarization curves for a wide range of operating conditions. Furthermore, the model is validated with experimental results from operating at 1–5 M of formic acid feed at 30–80 °C, and with Nafion-117 and silane-crosslinked sulfonated poly(styrene-ethylene/butylene-styrene) (sSEBS) membrane electrolytes reinforced in porous polytetrafluoroethylene (PTFE). The cell potential and power densities of experimental outcomes in direct formic acid fuel cells can be adequately predicted using the developed model.

Keywords: direct formic acid fuel cell; one-dimensional mathematical model; porous electrodes; cell potential; power density

1. Introduction

The research into fuel cell rockets has increased in the last decades, the direct formic acid fuel cells (DFAFCs) is considered to be a potential alternative power supply to the direct methanol fuel cell (DMFC), especially for portable electronic equipment [1]. The power necessity of portable electronic devices is 1–50 W to improve the power supply system with environmentally friendly and sustainable processes [2]. As a fuel, formic acid has numerous features that create a preferable anode feed in cell performance, rather than methanol- and hydrogen-based fuel cells [3]. The DFAFCs facilitates lower crossover flux through the electrolyte membrane than that of methanol, faster electrochemical kinetics due to the smaller molecular size than methanol, and non-toxicity [4]. In addition, it has many advantages, such as a low emission of pollutants, high energy density, and the aptitude to utilize liquid fuel that is more readily stored and transported than hydrogen fuel [5,6]. Moreover, a DFAFC has a higher theoretical cell potential (1.48 V), exhibiting a higher voltage output compared to that

in a methanol (1.21 V) and gaseous hydrogen cell (1.23 V), respectively [5,7]. Therefore, DFAFCs are expected to supply higher power density than DMFCs at ambient temperature, which is preferable for portable devices. Since the slow diffusion of the formic anion generated from the formic acid partial dissociation in aqueous medium, the formic acid crossover through the Nafion[®] 117 electrolyte membrane is decreased [8]. There is less electrode poisoning due to the dual path reaction of formic acid in a DFAFC [9]. Moreover, the proton conductivity of formic acid is expected to enhance the utilization of the anode electro-catalyst without introducing additional proton conductors into the anode catalyst [8]. These benefits make DFAFCs a potential power source.

Theoretical modeling with a comparison of experimental evidence on DFAFCs is important to predict the characterizing actual working principles, time involved in prototyping, and to recognize the outcomes of different designing factors on the fuel cell performance. It can also illuminate the electrochemical reactions and its complex mass transfer mechanism, which exist in these cell operations [10]. In light of the increasing importance of DFAFCs, a few studies have been conducted to predict DFAFC performance. Perales-Rondón et al. demonstrated the formic acid oxidation mechanism of different Pt single crystal electrodes using extensive density functional theory (DFT) calculations and the proposed theoretical values were validated with experimental results [11]. Recently, Reis et al. reported the system model and simulated this by using sub-routine development that made predictions through a wide variety of operating parameters, such as membrane thickness, electrode stoichiometry, pressure, temperature, current density and reference properties for DFAFC [12]. Ha et al. introduced an empirical model to demonstrate the cell performance difference between active and passive DFAFCs [13]. Gao et al. explain the formic acid oxidation mechanisms on Pt(111) electrodes under electrochemical methods using DFT calculations compared with the analogous gas-phase reaction for DFAFC [14]. Shaegh et al. proposed a three-dimensional numerical model to predict the cell performance of formic acid in a microfluidic fuel cell [15]. Wang et al. investigated formic acid electro-oxidation on a Pt/C catalyst and developed an impedance model by incorporating kinetic reactions to simulate the experimental impedance response [16]. Bauskar and Rice reported a 25% increase in the performance of a DFAFC after incorporating a 17.5 wt. % pore-former to increase the porosity of the anode catalyst layer [7]. However, fitting the theoretical modeling with the experimental results of the full cell-operating parameters are limited in the literature for direct formic acid fuel cell performance and the present work explains the applicability of DFAFC predictions.

In this study, an analytical model is developed to predict the performance of DFAFCs operating under various conditions. This model is derived from our previous literature report on DMFC [6]. The proposed model can adequately predict the cell potential and power density of DFAFCs as a function of current density by taking into consideration various formic acid concentrations, cell temperatures, and different solid electrolytes. The cell performance obtained from our one-dimensional model is validated with experimental data, and this result is believed to improve the estimation of the DFAFC system.

2. Model Development

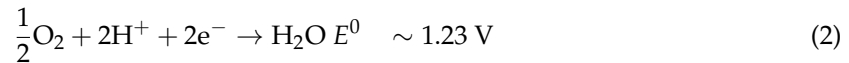
The proposed one-dimensional mathematical prediction of DFAFC is based on the Li et al. [17] and Kulikovskiy [18] proposed models and uses mass-transfer characteristics from analytical equations. Initially, we adopted the Lennard-Jones potential model [19], the Wilke-Chang estimation method [20], and the equation of state for a vapor-liquid equilibrium [21] to estimate the oxygen diffusion coefficients and formic acid in the fluids. According to Das et al.'s [22] formula, the diffusion coefficients were modified to calculate the effective diffusion coefficients of oxygen and formic acid in the porous diffusion electrodes. These diffusion coefficients were utilized to calculate the limiting current densities under different operating conditions. Finally, the Kulikovskiy [18] model is applied to predict the cell potential and to determine the power densities in a DFAFC using a 1–5 M formic acid feed from 30 °C to 80 °C, and Nafion and sulfonated block copolymer solid electrolytes. The developed one-dimensional mathematical model is demonstrated in the subsequent sections.

2.1. Conventional Model

Based on the polymeric electrolyte membrane for DFAFC, the O₂/air molecules passed in the cathode side and the formic acid fuel feed at the anode side by using a Pt-based electrocatalyst. The direct formic acid oxidation released two electrons per molecule from the anodic region and the reaction is:



Simultaneously, four electrons released per molecule by oxygen reduction in the cathode side reaction is:



The overall reaction of the anode and cathode in a DFAFC is as follows:



The assumptions for this model are described in the supplementary information.

The overpotential of a DFAFC is analogous to the DMFC model of Kulikovsky [18] and Li et al. [17] and can be described by the following equation:

$$V = E - \eta_a - \eta_\Omega - \eta_c \quad (4)$$

where η_a is the overpotential at the anode explained in Section 2.2, η_Ω is the ohmic potential drop in the electrolyte, which is assumed to be the major ohmic resistance contributor in the single cell, η_c is the overpotential at the cathode, explained in Section 2.4, and E is the thermodynamic potential of a DFAFC at a given operating condition.

The ohmic potential drop (η_Ω) is calculated as [18]:

$$\eta_\Omega = \frac{iL}{\sigma} \quad (5)$$

where σ is the ionic conductivity of the electrolyte, L is the thickness of membrane, and i is the current density.

For Nafion-117, the conductivity (σ) as a function of temperature (T) is described as follows:

$$\sigma = \sigma_{ref} \exp \left[1268 \left(\frac{1}{T_{ref}} - \frac{1}{T} \right) \right] \quad (6)$$

where σ_{ref} is the conductivity at a reference temperature (T_{ref}) [23] and has the value 0.05 S·cm⁻² [24]. The conductivity values of the silane-crosslinked sulfonated poly(styrene-ethylene/butylene-styrene) (sSEBS) were obtained from the literature [25–27].

According to the Nernst equation, the thermodynamic cell potential at any given condition (E) is:

$$E = E^0 - \frac{RT}{nF} \ln \frac{a_{\text{CO}_2} a_{\text{H}_2\text{O}}}{a_{\text{HCOOH}} a_{\text{O}_2}^{\frac{1}{2}}} \quad (7)$$

where R is the gas constant, F is Faraday's constant, T is the absolute temperature in Kelvin, n is the number of electrons in the half-reaction in a DFAFC (i.e., two), a is the activity of each product or reactant, and E^0 is the thermodynamic cell potential of the DFAFC under standard conditions (a pure substance at 25 °C and one bar). The thermodynamic cell potential (E^0) is calculated as:

$$E^0 = -\frac{\Delta G^0}{nF} \quad (8)$$

where ΔG^0 is the Gibbs free energy change of the formic acid oxidation reaction in Equation (3).

Once the cell voltage is determined at a specific current density, the predicted power density (P) of a DFAFC was calculated as the product of the predetermined current density and the estimated cell voltage (from Equation (4)):

$$P = iV \quad (9)$$

2.2. Anode Overpotential

The anode overpotential (η_a) can be calculated by the combination of the formic acid crossover, mass transport, and kinetic reactions, as illustrated in Equation (10) [17,28]:

$$\eta_a = b_a \ln\left(\frac{i}{i_{ea}}\right) - b_a \ln\left(1 - \frac{i}{i_{la}}\right) + b_a \ln(1 + \mu) \quad (10)$$

where μ is a dimensionless parameter related to the formic acid permeability (as defined in Equation (13)), and i is the experimental current density. The b_a and i_{ea} values are functions of temperature [29]:

$$b_a = \frac{RT}{0.8F} \quad (11)$$

where b_a is the Tafel slope at the anode and i_{ea} is the exchange current density at the anode:

$$i_{ea} = i_{ref} \left[\exp\left(\frac{24900}{8.314}\right) \left(\frac{1}{T_{ref}} - \frac{1}{T} \right) \right] \quad (12)$$

where i_{ref} is the exchange current density at 20 °C, whose value is 0.0014 (in A·m⁻²) [8]. The value of 24,900 (in J·mol⁻¹) is the activation energy derived by a linear regression of the data from the performance of a DFAFC [30].

The dimensionless parameter μ is calculated as:

$$\mu = \frac{\beta L_{ba}}{L D_{ba}} \quad (13)$$

where β is the formic acid permeability through the membrane with a thickness of L , D_{ba} is the effective diffusion coefficient of formic acid in aqueous solution (which is estimated using a procedure described in Section 2.3), and L_{ba} is the thickness of the anode diffusion layer. i_{la} is the limiting current density of the anode and it is defined as [18]:

$$i_{la} = 2F \frac{D_{ba} C_F}{L_{ba}} \quad (14)$$

where C_F is the concentration of the formic acid feed. In the anode half-reaction, because two electrons are produced for each formic acid molecule and transferred to the cathode, i.e., the proportional constant of two is used in Equation (14) [9].

2.3. Formic Acid Diffusion Coefficient at the Anode Electrode (D_{ba})

The formic acid diffusion coefficient in aqueous solution was estimated using the Darken equation [31,32]:

$$D_{FW} = (D_{FW}^\circ x_F + D_{WF}^\circ x_W) \alpha \quad (15)$$

where D_{FW} is the formic acid diffusion coefficient in water, D_{IJ}° is the diffusion coefficient of the solute I in an infinitely dilute solution of solvent J , and F and W denote formic acid and water, respectively. The variables x_F and x_W are the formic acid and water molar fractions, respectively.

The parameter α is a thermodynamic correction term given by the following equation [33]:

$$\alpha = \left(\frac{\partial \ln a_F}{\partial \ln x_F} \right)_{T,P} \quad (16)$$

where a_F and x_F are the activity and mole fraction of formic acid, respectively, in the binary formic acid/water solution. The values of D_{FW}° and D_{WF}° were predicted using the Wilke-Chang equation for the diffusion coefficients of solutes in solvents at infinite dilution [20]:

$$D_W = \frac{7.4 \times 10^{-8} (\Phi_F M_F)^{1/2} T}{\zeta_F v_W^{0.6}} \quad (17)$$

and:

$$D_{FW}^\circ = \frac{7.4 \times 10^{-8} (\Phi_W M_W)^{1/2} T}{\zeta_W v_F^{0.6}} \quad (18)$$

where T is the temperature, M is the solvent molecular weight, v is the solute molar volume at its boiling temperature, ζ is the solvent viscosity [34], and Φ is the association factor of the solvent (2.6 for water and one for formic acid [20]). The correction term α in Equation (16) was acquired from the vapor-liquid equilibrium data of formic acid and water [21] using Universal quasichemical (UNIQUAC) parameters.

By substituting appropriate formic acid concentrations and temperatures, we obtained the corresponding formic acid diffusion coefficients in water. Then, the effective formic acid diffusion coefficient in the porous diffusion layer was calculated as [22,35]:

$$D_{FW}^{\text{eff}} = \left(1 - \left(\frac{3(1 - \theta_a)}{3 - \theta_a} \right) \right) D_{FW} \quad (19)$$

where θ_a is the porosity of the anode diffusion layer. The experimental methanol diffusion coefficient at 90 °C has been reported to be $1.8 \times 10^{-5} \text{ cm}^2 \text{ s}^{-1}$ with a b_a of 0.3 mm [18]. This value was used to calculate the apparent porosity θ_a (which was estimated to be 0.406). The predicted effective formic acid diffusion coefficient was used as D_{ba} in Equations (13) and (14) to estimate the anode overpotential described in Section 2.2.

2.4. Cathode Overpotential

The cathode overpotential (η_c) caused by the diffusional mass-transfer limitation due to a loss in oxygen concentration can be predicted from the combination of the formic acid crossover, mass transport, and kinetic reaction using the following equation:

$$\eta_c = b_c \ln\left(\frac{i}{i_{ec}}\right) - b_c \ln\left(1 - \frac{i}{i_{lc}} - R_C\right) \quad (20)$$

where i_{lc} is the limiting current density at the cathode, i_{ec} is the exchange current density of the cathode, b_c is the Tafel slope at the cathode, and R_C is a dimensionless parameter accounting for the potential drop due to the formic acid crossover. The b_c and i_{ec} values depend on the cell temperature [36]:

$$b_c = \frac{RT}{0.7F} \quad (21)$$

and:

$$i_{ec} = 0.04222 \left[\exp\left(\frac{73200}{8.314}\right) \left(\frac{1}{273 + 80} - \frac{1}{T} \right) \right] \quad (22)$$

This correlation depends on an activation energy of 73,200 J·mol⁻¹, conducted between 30 and 80 °C using Nafion-117 sandwiched between Pt microelectrodes [37].

The R_c value was obtained using the following equation:

$$R_c = \frac{i_{la}}{i_{lc}} \left(\frac{\mu}{1 + \mu} \right) \left(1 - \frac{i}{i_{la}} \right) \quad (23)$$

where μ is a dimensionless parameter (defined in Equation (13)), i_{la} is the limiting current density at the anode (defined in Equation (14)), and i_{lc} is the limiting current density at the cathode. The i_{lc} value was obtained using the following equation:

$$i_{lc} = 4F \frac{D_{bc} C_O}{L_{bc}} \quad (24)$$

where D_{bc} is the oxygen diffusion coefficient in the cathode backing layer (detailed in the supplementary information), L_{bc} is the thickness of the cathode backing layer and C_O is the oxygen feed concentration.

The modeling of the oxygen diffusion coefficient into the cathode is described in [6] and the details are described in the supplementary information.

3. Experimental Section

3.1. Electrolyte Preparation

The Nafion-117 membrane (from DuPont Co., Fayetteville, NC, USA) was first heated with hydrogen peroxide (5 wt. %) for 1 h to remove organic residuals and then soaked in deionized (DI) water for 30 min. Afterward, the Nafion membrane was heated in sulfuric acid (1 M) for 1 h to assemble a complete exchange to a proton-type ionic exchange membrane and again soaked with DI water. Microporous polytetrafluoroethylene (PTFE) film was immersed in a 5% silane-crosslinked sulfonated poly(styrene-ethylene/butylene-styrene) (sSEBS) solution and degassed for 15 min to allow the sSEBS solution to fill the polytetrafluoroethylene (PTFE) pores. Thus, the sSEBS matrix was reinforced by the PTFE film. The wet composite electrolyte was heated in a vacuum oven at 120 °C for 12 h and exposed to UV light (500 W) for 2 h on both sides of the PTFE to cross-linking the sSEBS. The dried sSEBS/PTFE composite was soaked in 1 M sulfuric acid at 60 °C for 1 h and soaked with DI water.

3.2. Conductivity and Formic Acid Permeability Measurements

The electrolyte membrane was immersed in DI water and formic acid solutions at different temperatures for 3 h and placed between two stainless steel electrode rods in a T-tube glass, as illustrated in our previous report [38–40]. The membrane was maintained at 98% relative humidity at a fixed temperature for the proton conductivity analysis. An alternate-current impedance spectrum was attained using a potentiostat (PGSTAT-30, MetrohmAutolab B.V., Utrecht, The Netherlands). Nyquist plots were employed to analyze the conductivity of the electrolytic membrane, as illustrated in our previous work [38,41].

The formic acid permeability was studied using a hand-made glass permeation cell. The permeation cell was separated into two compartments. One compartment was filled with a formic acid with DI water, and the other receiving compartment was filled with DI water. The electrolytic membrane was positioned between these two compartments, and the formic acid transport through the membrane was analyzed with time. The gas chromatograph (HP 4890A, Agilent Technologies Co. Ltd., St. Louis, MO, USA) was used to analyze the formic acid concentration. The calculations and experimental set-up of the formic acid permeability were illustrated in our previous reports [42,43].

3.3. Formic Acid Fuel Cell Test

The electrolytic membrane (Nafion-117 or sSEBS/PTFE) was sandwiched between the sheets of the gas diffusion electrodes (from E-tek, 6 mg·cm⁻² Pt-Ru for the anode and 5 mg·cm⁻² Pt for the cathode) to form a membrane electrode assembly (MEA). The active area of the MEA was 5 cm².

Two flow-field plates with carved double-channel serpentine flow paths (1 mm wide and 1 mm deep) were placed next to the MEA. Next to the flow-field plates, two gold-plated copper end plates were used as current collectors and assembled. For temperature control, two heating tapes were adhered to the end plate surfaces [38]. The humidified oxygen gas was fed into the cathode (flow rate of $180 \text{ mL}\cdot\text{min}^{-1}$), and the thermostated formic acid solution was fed into the anode side (flow rate of $3 \text{ mL}\cdot\text{min}^{-1}$). A thermocouple was placed into the end plates, and the analyzed temperature was fed to a controller to confirm that the cell temperature was at the set point. The electrochemical analysis of the DFAFCs were measured using a constant current density mode with a potentiostat (PGSTAT-30, MetrohmAutolab B.V., Utrecht, The Netherlands). The experimental set-up of the single cell performance was described in previous reports [38,39,44,45]. The different parameters of cell temperature ranged from $30 \text{ }^\circ\text{C}$ to $80 \text{ }^\circ\text{C}$ and a formic acid concentration from 1 M to 5 M. In the first set of experiments (1–2 M), the voltage lower limit was set at 0.45 V, but was changed to 0.1–0.2 V in subsequent experiments.

4. Results and Discussion

The thermodynamic correction term of α in Equation (16) from the Section 2.3 was acquired from the vapor–liquid equilibrium data of formic acid and water [21] using universal quasi-chemical (UNIQUAC) parameters. The values of $\ln a_F$ and $\ln x_F$ from $30 \text{ }^\circ\text{C}$ to $80 \text{ }^\circ\text{C}$ are plotted in Figure 1. From the slope, we obtained α values of 2.1769, 2.1743, 2.1715, and 2.1652 for 1 M, 2 M, 3 M, and 5 M formic acid solutions, respectively, at $30 \text{ }^\circ\text{C}$. For instance, the α values were 1.8698, 1.8747, 1.8797, and 1.8895 for 1 M, 2 M, 3 M, and 5 M formic acid solutions, respectively, at $80 \text{ }^\circ\text{C}$. The slight decreases in α values as the temperature increases are due to the methanol/water binary mixture at an elevated temperature close to an ideal solution, with the vapor-liquid equilibrium predictable using Raoult's law [33]. Once this value was determined, the formic acid diffusivity in water was predictable for a certain composition by applying Equation (15) from Section 2.3.

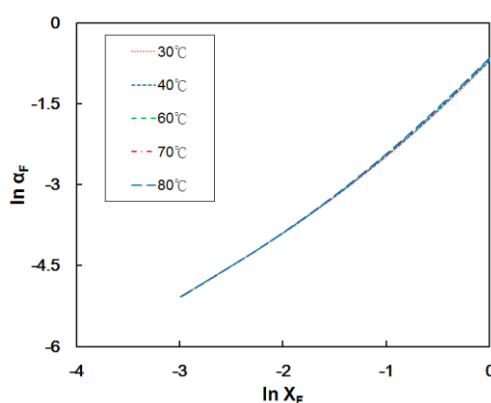


Figure 1. Plots of $\ln a_F$ versus $\ln x_F$ for formic acid solutions at $30\text{--}80 \text{ }^\circ\text{C}$. The slope at any formic acid mole fraction corresponds to the α value defined in Equation (16) from Section 2.3.

4.1. Effect of Temperature on Fuel Cell Performance Using the Modified Model

The proposed mathematical model for DFAFC performance was compared with the experimental data collected at $40 \text{ }^\circ\text{C}$ to $80 \text{ }^\circ\text{C}$ using a Nafion-117 membrane and a 1 M formic acid as the anode feed. The predicted cell voltage and current density data for the Nafion-117 membrane at $40\text{--}80 \text{ }^\circ\text{C}$ are shown in Figure 2a. At $40 \text{ }^\circ\text{C}$, the current density of the experimental value was slightly deviated ($\sim 1\%$) from the theoretical modeling data. This was due to the fact that the initial electrochemical reaction between the electrodes and membrane electrolyte was not enough to transfer the protons efficiently. However, further increasing the temperature at 60 to $80 \text{ }^\circ\text{C}$, the experimental current density values were exactly matched with the corresponding theoretical prediction due to an improved electrochemical reaction and mass

transfer phenomenon. In addition, the full cell polarization curve was obtained as a linear curve due to the reduction of the ohmic resistance and increase of the ionic conductivity. When increasing the temperature, the current density also increased from 98 to 228 $\text{mA}\cdot\text{cm}^{-2}$, respectively within the voltage range.

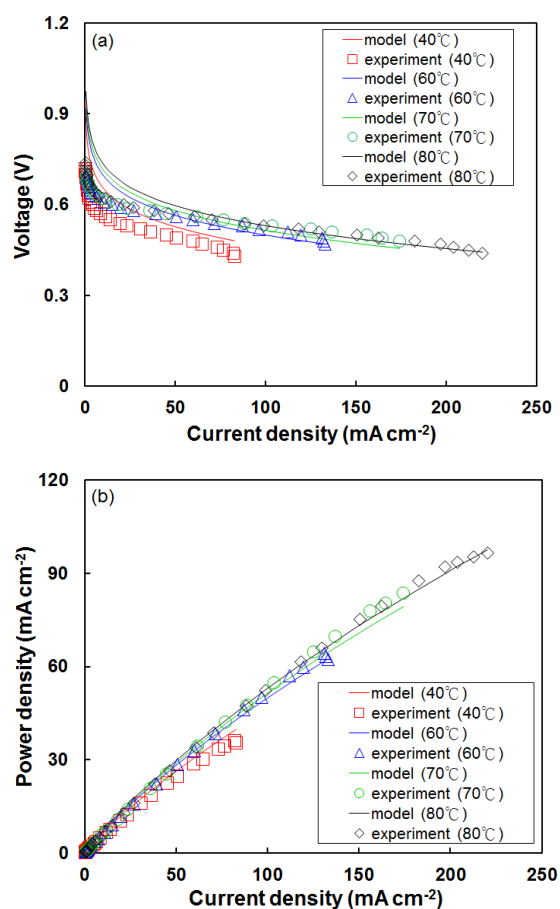


Figure 2. Predicted (a) polarization curves and (b) power densities for direct formic acid fuel cells (DFAFCs) at various operating temperatures, along with experimental data. The cell was fed with a 1 M formic acid solution, humidified oxygen, and equipped with a Nafion-117 electrolyte.

Similarly, the cell temperature increased from 40 °C to 80 °C, and the power density was also increased from 24.6 to 96.6 $\text{mW}\cdot\text{cm}^{-2}$. The increasing power density values resulted from the higher Nafion-117 conductivity associated with a higher temperature, leading to a slower decline in ohmic loss (Figure 2a). The result confirms that by increasing the temperature, the efficiency of the power densities was also increased due to the activation overpotential produced in the electrolyte membrane [12]. The predicted power density data using the modified model were in excellent agreement with the experimental results for the entire temperature range. One of the main contributions of this approach is the ability to predict the DFAFC performance at different temperatures, given the availability of the diffusion layer porosity data. Other determinations are based on theoretical mass-transfer equations. By assuming that the porosities are not significantly affected by the temperature change, the porosity values can be used to estimate the effective diffusivity at other temperatures using the procedure outlined in Section 2.3.

4.2. Effect of Formic Acid Concentration on Cell Performance Using the Modified Model

The estimated polarization curves and the power densities for DFAFCs fed with different formic acid feed concentrations at 70 °C and equipped with Nafion-117 membrane are illustrated in Figure 3b. The measured formic acid permeability data from the aqueous solutions of various concentrations were

7.77×10^{-6} , 8.15×10^{-6} , 8.52×10^{-6} , and $1.25 \times 10^{-5} \text{ cm}^2 \cdot \text{s}^{-1}$ for 1 M, 2 M, 3 M, and 5 M, respectively, at 70 °C. The results confirm that lower formic acid feeds suppressed the permeability than higher anode feed concentrations. The formic acid permeability has the same magnitude as the permeability of methanol in Nafion-117 [8,46]. The estimated P_{max} values for 3 M, and 5 M anode feeds were 157, and 168 $\text{mW} \cdot \text{cm}^{-2}$ at 70 °C, respectively. The reason for increasing P_{max} is mainly ascribed to the improved kinetics of the formic acid electro-oxidation reaction that can reduce the fuel crossover from anode to cathode at higher feed concentrations. Compared with the experimental data under similar conditions, in which the P_{max} values were 150, and 176 $\text{mW} \cdot \text{cm}^{-2}$ at their corresponding formic acid concentrations, the proposed model was able to predict enhanced cell voltage and power density with increasing formic acid concentration. The theoretical and experimental deviation of P_{max} values for 3 M and 4 M anode feeds were 4.5% and 4.6%, respectively. On average, the modified model predictions deviated by approximately 4.5% from the experimental data. Krishnamurthy et al. reported the computation modeling of fuel cell values have a maximum deviation of 19% when compared to experimental results with different operating parameters. The deviation occurred due to uncertainty in the kinetics and mass transfer parameters, a higher degree of anisotropy, a cross-over phenomenon and a wide range of pore sizes [10]. This model can provide reasonable DFAFC performance predictions for a wide range of formic acid concentrations. Therefore, the modified model of theoretical prediction of polarization curves and power density was more profound in the experimental analysis via anode feed concentrations.

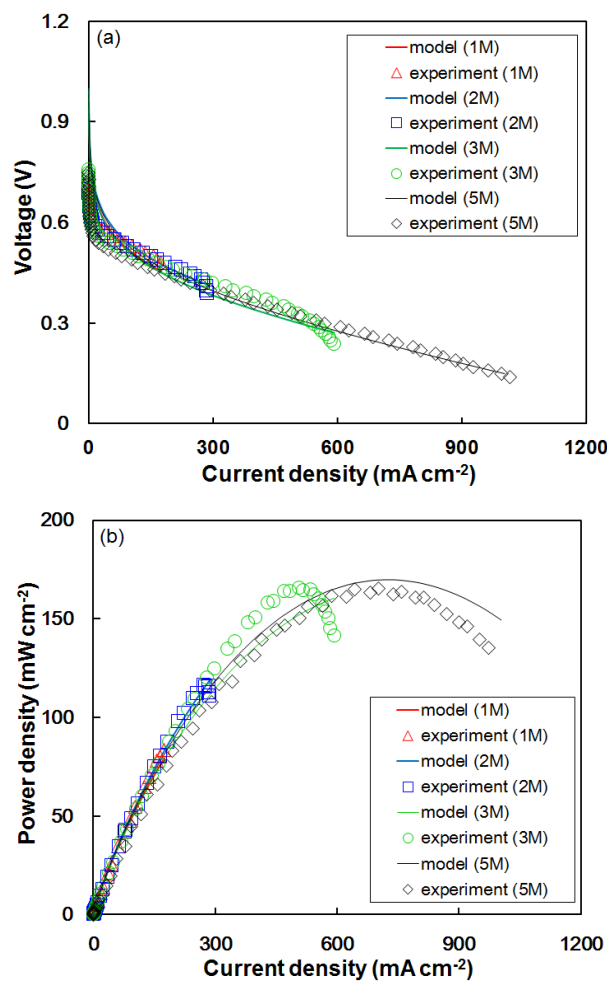


Figure 3. Predicted (a) polarization curves and (b) power density results for DFAFCs fed with various formic acid concentrations, along with experimental data. The DFAFCs were operated at 70 °C.

4.3. Modeling for sSEBS/PTFE Membrane Electrolytes

The DFAFC experimental results using the sSEBS/PTFE composite were used to verify the versatility of the modified model. This electrolyte membrane was fabricated and characterized in our laboratory. The estimated DFAFC voltage and power density data using the sSEBS/PTFE with 1 M formic acid feeds at 30 °C and 60 °C are shown in Figure 4a,b, respectively. The performance predictions were in accordance with the experimental data. With a 1 M formic acid feed at 30 °C, the estimated P_{\max} using the sSEBS/PTFE electrolyte was $28 \text{ mW}\cdot\text{cm}^{-2}$, which is approximately the experimental result of $25 \text{ mW}\cdot\text{cm}^{-2}$. For the 60 °C formic acid feed, the P_{\max} prediction was $63 \text{ mW}\cdot\text{cm}^{-2}$, in agreement with the experimental value of $55 \text{ mW}\cdot\text{cm}^{-2}$. The predicted peak power densities for both conditions at 30 °C and 60 °C are higher by 12–15% than the experimental results. The deviation between the experimental data and predicted values were probably due to the variation in the Tafel slope of formic acid oxidation. The literature data [47,48] were not carried out under identical conditions (such as temperature, mole concentration, etc.) and measured with acid (HCl or H_2SO_4) on a Pt/C catalyst. No acid was fed to the anode and Pt-Ru/C catalyst was employed in our formic acid fuel cells. These differences may contribute uncertainty to estimating the anode overpotential. We adopted the value in this work from a recently published article [29] for the simulation.

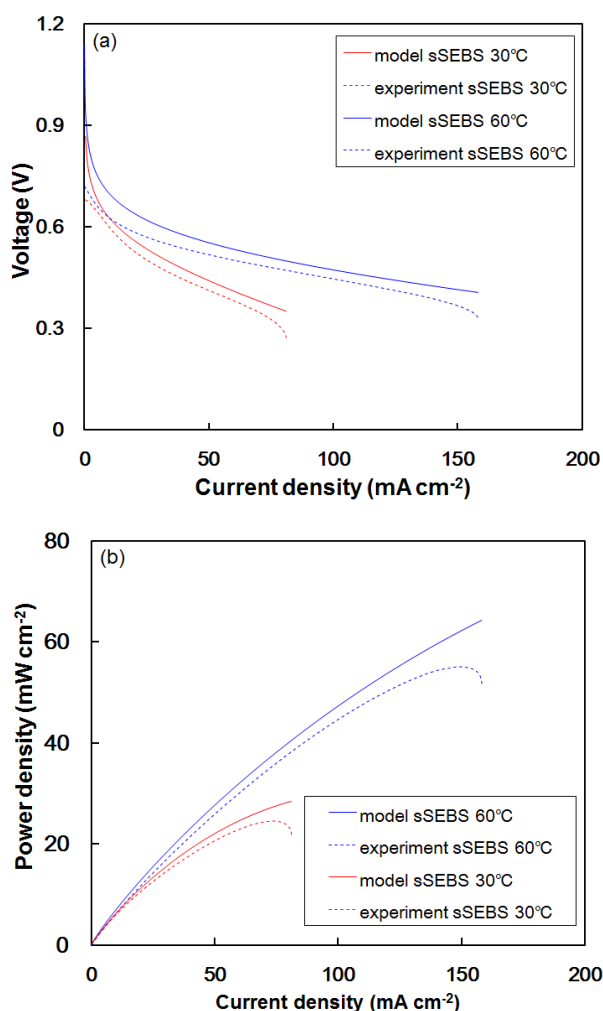


Figure 4. Predicted (a) polarization curves and (b) power density results for DFAFCs equipped with silane-crosslinked sulfonated poly(styrene-ethylene/butylene-styrene)/ porous polytetrafluoroethylene (sSEBS/PTFE) electrolyte. The DFAFCs were fed with a 1 M formic acid solution and humidified oxygen, and they were operated at 30 °C and 60 °C.

The results mentioned above demonstrate that given the electrolyte characteristics (thickness, conductivity, and formic acid permeability), operating conditions (temperature, feed concentration, electrode porosity), and associated reactant mass-transfer properties (viscosity, molar volume), one can apply our modified model to estimate the DFAFC performance. This modeling process provides cost-saving advantages by eliminating unnecessary testing of different fuel cell preparations, which would require the usage of expensive catalysts and electrolytes. Preliminary data on fuel cell performance can be simulated with sufficient precision using this model. Further work can be performed to expand the usage of this model to other operating conditions (e.g., using a Tafel slope for another catalyst) by changing appropriate variables outlined in the Section 2.

5. Conclusions

The effective diffusion coefficients of the reactants in the porous diffusion layer were estimated using the Wilke–Chang equation, the Lennard–Jones potential model, and the UNIQUAC equation for the vapor–liquid equilibrium data on formic acid/water solutions. The data were adopted into a modified Kulikovsky model to estimate the polarization curve and power density of a DFAFC. Therefore, the prediction has a theoretical basis without the requirement of any fitting parameters. The model was validated using experimental results obtained with 1 M–5 M formic acid feeds and operating temperatures at 30–80 °C with Nafion and other solid electrolytes. This model was able to predict the effects of the diffusion layer porosity, cell temperature, and formic acid concentration on cell performance using various electrolyte membranes. The simulation model provides a valuable development tool that possesses cost- and time-saving advantages for researchers. In addition, the developed theoretical modeling is valuable for both scientific thoughts and performance predictions to achieve a clear appreciation of the interplay between various physicochemical and electrochemical mechanisms for the effect on DFAFC performance.

Supplementary Materials: Supplementary materials can be accessed at: <http://www.mdpi.com/1996-1073/10/12/1972/s1>.

Acknowledgments: The authors acknowledge the financial support from the Ministry of Science and Technology (MOST-106-2221-E-182-051-MY3) and Chang Gung Memorial Hospital (CMRPD2F0052).

Author Contributions: Shingjiang Jessie Lue and Nai-Yuan Liu conceived and designed the experiments and theoretical analysis and the fuel cell performance; Selvaraj Rajesh Kumar and Shingjiang Jessie Lue contributes the all data analysis and wrote the paper; Kevin Chi-Yang Tseng, Bo-Yan Wang and Chieh-Hsin Leung contributed the preparation of the electrolytic membrane and data analysis. All authors examined and approved the final manuscript.

Conflicts of Interest: The authors declare no conflict of interest.

Nomenclature

a	activity of reactant or product (–)
b_a	Tafel slope at the anode (V)
b_c	Tafel slope at the cathode (V)
C_O	oxygen concentration ($\text{mol}\cdot\text{cm}^{-3}$)
C_F	formic acid concentration ($\text{mol}\cdot\text{cm}^{-3}$)
D_{ba}	formic acid diffusion coefficient in the anode diffusion layer ($\text{cm}^2\cdot\text{s}^{-1}$)
D_{bc}	oxygen diffusion coefficient in the cathode diffusion layer ($\text{cm}^2\cdot\text{s}^{-1}$)
D°	solute diffusion coefficient at infinite dilution ($\text{cm}^2\cdot\text{s}^{-1}$)
D^{eff}	effective diffusion coefficient of reactant in the porous diffusion layer ($\text{cm}^2\cdot\text{s}^{-1}$)
D_{IJ}	diffusion coefficient of component I in mixture with J ($\text{cm}^2\cdot\text{s}^{-1}$)
E^0	thermodynamic cell potential at standard state (V)
E	thermodynamic cell potential at any condition (V)
F	Faraday's constant ($96,485\text{ C}\cdot\text{mol}^{-1}$)
ΔG^0	Gibbs free energy change in overall reaction for a DFAFC at standard state ($\text{J}\cdot\text{mol}^{-1}$)
i_{ec}	exchange current density for the cathode ($\text{A}\cdot\text{cm}^{-2}$)

Nomenclature

i_{ea}	exchange current density for the anode ($A \cdot cm^{-2}$)
i	current density ($A \cdot cm^{-2}$)
i_{lc}	limiting current density at the cathode ($A \cdot cm^{-2}$)
i_{la}	limiting current density at the anode ($A \cdot cm^{-2}$)
L	thickness of the electrolyte (cm)
L_{bc}	thickness of backing layer at the cathode (cm)
L_{ba}	thickness of backing layer at the anode (cm)
M	molar mass ($g \cdot mol^{-1}$)
n	number of electrons in half-reaction
p	gas pressure (bar)
P	power density ($mW \cdot cm^{-2}$)
R_c	dimensionless parameter accounting for potential drop due to formic acid crossover (–)
R	gas constant ($8.314 J \cdot mol^{-1} \cdot K^{-1}$)
T^*	reduced temperature (–)
T	temperature (K)
v	molar volume (cm^3)
V	cell voltage (V)
x	mole fraction (–)
<i>Greek</i>	
α	thermodynamic correction term (–)
β	formic acid permeability ($cm^2 \cdot s^{-1}$)
ε	characteristic Lennard-Jones energy (J)
ζ	solvent viscosity (cP)
η_{Ω}	ohmic potential drop (V)
η_a	overpotential at the anode (V)
η_c	overpotential at the cathode (V)
θ	porosity of diffusion layer (–)
Φ	solvent association constant (–)
κ	Boltzmann's constant ($J \cdot K^{-1}$)
μ	dimensionless parameter (–)
σ	proton conductivity of the solid electrolyte membrane ($S \cdot m^{-1}$)
σ_{OA}	characteristic Lennard-Jones length (Å)
Ω_D	diffusion collision integral (–)

References

- Zhu, Y.; Ha, S.Y.; Masel, R.I. High power density direct formic acid fuel cells. *J. Power Sources* **2004**, *130*, 8–14. [[CrossRef](#)]
- Sebastian, D.; Serov, A.; Matanovic, I.; Artyushkova, K.; Atanassov, P.; Arico, A.; Baglio, V. Insights on the extraordinary tolerance to alcohols of Fe-NC cathode catalysts in highly performing direct alcohol fuel cells. *Nano Energy* **2017**, *34*, 195–204. [[CrossRef](#)]
- Mohammad, A.M.; El-Nagar, G.A.; Al-Akraa, I.M.; El-Deab, M.S.; El-Anadouli, B.E. Towards improving the catalytic activity and stability of platinum-based anodes in direct formic acid fuel cells. *Int. J. Hydrog. Energy* **2015**, *40*, 7808–7816. [[CrossRef](#)]
- Baik, S.; Kim, J.; Han, J.; Kwon, Y. Performance improvement in direct formic acid fuel cells (DFAFCs) using metal catalyst prepared by dual mode spraying. *Int. J. Hydrog. Energy* **2011**, *36*, 12583–12590. [[CrossRef](#)]
- Yu, X.; Pickup, P.G. Recent advances in direct formic acid fuel cells (DFAFC). *J. Power Sources* **2008**, *182*, 124–132. [[CrossRef](#)]
- Wang, B.-Y.; Lin, H.-K.; Liu, N.-Y.; Mahesh, K.; Lue, S.J. Cell performance modeling of direct methanol fuel cells using proton-exchange solid electrolytes: Effective reactant diffusion coefficients in porous diffusion layers. *J. Power Sources* **2013**, *227*, 275–283. [[CrossRef](#)]

7. Bauskar, A.S.; Rice, C.A. Impact of anode catalyst layer porosity on the performance of a direct formic acid fuel cell. *Electrochim. Acta* **2012**, *62*, 36–41. [[CrossRef](#)]
8. Jiang, J.; Kucernak, A. Probing anodic reaction kinetics and interfacial mass transport of a direct formic acid fuel cell using a nanostructured palladium–gold alloy microelectrode. *Electrochim. Acta* **2009**, *54*, 4545–4551. [[CrossRef](#)]
9. Rice, C.; Ha, S.; Masel, R.; Waszczuk, P.; Wieckowski, A.; Barnard, T. Direct formic acid fuel cells. *J. Power Sources* **2002**, *111*, 83–89. [[CrossRef](#)]
10. Krishnamurthy, D.; Johansson, E.O.; Lee, J.W.; Kjeang, E. Computational modeling of microfluidic fuel cells with flow-through porous electrodes. *J. Power Sources* **2011**, *196*, 10019–10031. [[CrossRef](#)]
11. Perales-Rondón, J.V.; Herrero, E.; Feliu, J.M. On the activation energy of the formic acid oxidation reaction on platinum electrodes. *J. Electroanal. Chem.* **2015**, *742*, 90–96. [[CrossRef](#)]
12. Reis, A.; Mert, S.O. Performance assessment of a direct formic acid fuel cell system through exergy analysis. *Int. J. Hydrog. Energy* **2015**, *40*, 12776–12783. [[CrossRef](#)]
13. Ha, S.; Dunbar, Z.; Masel, R. Characterization of a high performing passive direct formic acid fuel cell. *J. Power Sources* **2006**, *158*, 129–136. [[CrossRef](#)]
14. Gao, W.; Keith, J.A.; Anton, J.; Jacob, T. Theoretical elucidation of the competitive electro-oxidation mechanisms of formic acid on Pt (111). *J. Am. Chem. Soc.* **2010**, *132*, 18377–18385. [[CrossRef](#)] [[PubMed](#)]
15. Shaegh, S.A.M.; Nguyen, N.-T.; Chan, S.H. An air-breathing microfluidic formic acid fuel cell with a porous planar anode: Experimental and numerical investigations. *J. Micromech. Microeng.* **2010**, *20*, 105008. [[CrossRef](#)]
16. Wang, X.; Hu, J.-M.; Hsing, I.-M. Electrochemical investigation of formic acid electro-oxidation and its crossover through a Nafion[®] membrane. *J. Electroanal. Chem.* **2004**, *562*, 73–80. [[CrossRef](#)]
17. Li, X.; Roberts, E.; Holmes, S. Evaluation of composite membranes for direct methanol fuel cells. *J. Power Sources* **2006**, *154*, 115–123. [[CrossRef](#)]
18. Kulikovskiy, A. A method for analysis of DMFC performance curves. *Electrochem. Commun.* **2003**, *5*, 1030–1036. [[CrossRef](#)]
19. Hirschfelder, J.; Bird, R.B.; Curtiss, C.F. *Molecular Theory of Gases and Liquids*; Wiley: New York, NY, USA, 1964.
20. Wilke, C.; Chang, P. Correlation of diffusion coefficients in dilute solutions. *AIChE J.* **1955**, *1*, 264–270. [[CrossRef](#)]
21. Smith, J.M.; Van Ness, H.C.; Abbott, V.N. *Introduction to Chemical Engineering Thermodynamics*; McGraw-Hill Book: Boston, MA, USA, 2005.
22. Das, P.K.; Li, X.; Liu, Z.-S. Effective transport coefficients in PEM fuel cell catalyst and gas diffusion layers: Beyond Bruggeman approximation. *Appl. Energy* **2010**, *87*, 2785–2796. [[CrossRef](#)]
23. Nguyen, T.V.; White, R.E. A water and heat management model for Proton-Exchange-Membrane fuel cells. *J. Electrochem. Soc.* **1993**, *140*, 2178–2186. [[CrossRef](#)]
24. Alberti, G.; Casciola, M. Solid state protonic conductors, present main applications and future prospects. *Solid State Ion.* **2001**, *145*, 3–16. [[CrossRef](#)]
25. Weiss, R.; Sen, A.; Willis, C.; Pottick, L. Block copolymer ionomers: 1. Synthesis and physical properties of sulphonated poly (styrene-ethylene/butylene-styrene). *Polymer* **1991**, *32*, 1867–1874. [[CrossRef](#)]
26. Won, J.; Choi, S.W.; Kang, Y.S.; Ha, H.Y.; Oh, I.-H.; Kim, H.S.; Kim, K.T.; Jo, W.H. Structural characterization and surface modification of sulfonated polystyrene-(ethylene-butylene)-styrene triblock proton exchange membranes. *J. Membr. Sci.* **2003**, *214*, 245–257. [[CrossRef](#)]
27. Kim, B.; Kim, J.; Jung, B. Morphology and transport properties of protons and methanol through partially sulfonated block copolymers. *J. Membr. Sci.* **2005**, *250*, 175–182. [[CrossRef](#)]
28. Divisek, J.; Fuhrmann, J.; Gärtner, K.; Jung, R. Performance modeling of a direct methanol fuel cell. *J. Electrochem. Soc.* **2003**, *150*, A811–A825. [[CrossRef](#)]
29. Liu, Y.; Wang, Y.; Deng, C.; Wu, B.; Gao, Y. Kinetic study of formic acid oxidation on carbon supported platinum electrocatalyst. *Electrochemistry* **2010**, *78*, 662–665. [[CrossRef](#)]
30. Velázquez-Palenzuela, A.; Centellas, F.; Garrido, J.A.; Arias, C.; Rodríguez, R.M.; Brillas, E.; Cabot, P.-L. Kinetic analysis of carbon monoxide and methanol oxidation on high performance carbon-supported Pt–Ru electrocatalyst for direct methanol fuel cells. *J. Power Sources* **2011**, *196*, 3503–3512. [[CrossRef](#)]
31. Darken, L.S. Diffusion, mobility and their interrelation through free energy in binary metallic system. *Trans. Am. Inst. Min. Metall. Eng.* **1948**, *175*, 184.

32. Ghai, R.; Ertl, H.; Dullien, F. Liquid diffusion of nonelectrolytes: Part I. *AIChE J.* **1973**, *19*, 881–900. [[CrossRef](#)]
33. Reid, R.C.; Prausnitz, J.; Poling, B. *The Properties of Gases and Liquids*; McGraw-Hill: New York, NY, USA, 1987; Volume 4.
34. Yang, C.; Wei, G.; Li, Y. Densities and Viscosities of *N,N*-Dimethylformamide+ Formic Acid, and+ Acetic Acid in the Temperature Range from (303.15 to 353.15) K. *J. Chem. Eng. Data* **2008**, *53*, 1211–1215. [[CrossRef](#)]
35. Zamel, N.; Astrath, N.G.; Li, X.; Shen, J.; Zhou, J.; Astrath, F.B.; Wang, H.; Liu, Z.-S. Experimental measurements of effective diffusion coefficient of oxygen–nitrogen mixture in PEM fuel cell diffusion media. *Chem. Eng. Sci.* **2010**, *65*, 931–937. [[CrossRef](#)]
36. Wang, Z.; Wang, C. Mathematical modeling of liquid-feed direct methanol fuel cells. *J. Electrochem. Soc.* **2003**, *150*, A508–A519. [[CrossRef](#)]
37. Parthasarathy, A.; Srinivasan, S.; Appleby, A.J.; Martin, C.R. Temperature dependence of the electrode kinetics of oxygen reduction at the platinum/Nafion[®] interface—A microelectrode investigation. *J. Electrochem. Soc.* **1992**, *139*, 2530–2537. [[CrossRef](#)]
38. Lue, S.J.; Wang, W.-T.; Mahesh, K.; Yang, C.-C. Enhanced performance of a direct methanol alkaline fuel cell (DMAFC) using a polyvinyl alcohol/fumed silica/KOH electrolyte. *J. Power Sources* **2010**, *195*, 7991–7999. [[CrossRef](#)]
39. Rajesh Kumar, S.; Juan, C.-H.; Liao, G.-M.; Lin, J.-S.; Yang, C.-C.; Ma, W.-T.; You, J.-H.; Jessie Lue, S. Fumed silica nanoparticles incorporated in quaternized poly (vinyl alcohol) nanocomposite membrane for enhanced power densities in direct alcohol alkaline fuel cells. *Energies* **2016**, *9*, 15. [[CrossRef](#)]
40. Lin, J.-S.; Ma, W.-T.; Shih, C.-M.; Yu, B.-C.; Teng, L.-W.; Wang, Y.-C.; Cheng, K.-W.; Chiu, F.-C.; Lue, S.J. Reorientation of magnetic graphene oxide nanosheets in crosslinked quaternized polyvinyl alcohol as effective solid electrolyte. *Energies* **2016**, *9*, 1003. [[CrossRef](#)]
41. Rajesh Kumar, S.; Ma, W.-T.; Lu, H.-C.; Teng, L.-W.; Hsu, H.-C.; Shih, C.-M.; Yang, C.-C.; Lue, S.J. Surfactant-Assisted Perovskite Nanofillers Incorporated in Quaternized Poly (Vinyl Alcohol) Composite Membrane as an Effective Hydroxide-Conducting Electrolyte. *Energies* **2017**, *10*, 615. [[CrossRef](#)]
42. Lue, S.J.; Juang, H.J.; Hou, S.Y. Permeation of xylene isomers through supported liquid membranes containing cyclodextrins. *Sep. Sci. Technol.* **2002**, *37*, 463–480. [[CrossRef](#)]
43. Lue, S.J.; Shih, T.-S.; Wei, T.-C. Plasma modification on a Nafion membrane for direct methanol fuel cell applications. *Korean J. Chem. Eng.* **2006**, *23*, 441–446. [[CrossRef](#)]
44. Lue, S.J.; Mahesh, K.; Wang, W.-T.; Chen, J.-Y.; Yang, C.-C. Permeant transport properties and cell performance of potassium hydroxide doped poly (vinyl alcohol)/fumed silica nanocomposites. *J. Membr. Sci.* **2011**, *367*, 256–264. [[CrossRef](#)]
45. Lin, J.-S.; Kumar, S.R.; Ma, W.-T.; Shih, C.-M.; Teng, L.-W.; Yang, C.-C.; Lue, S.J. Gradiently distributed iron oxide@ graphene oxide nanofillers in quaternized polyvinyl alcohol composite to enhance alkaline fuel cell power density. *J. Membr. Sci.* **2017**, *543*, 28–39. [[CrossRef](#)]
46. Gold, S.; Chu, K.-L.; Lu, C.; Shannon, M.A.; Masel, R.I. Acid loaded porous silicon as a proton exchange membrane for micro-fuel cells. *J. Power Sources* **2004**, *135*, 198–203. [[CrossRef](#)]
47. Jiang, J.; Kucernak, A. Nanostructured platinum as an electrocatalyst for the electrooxidation of formic acid. *J. Electroanal. Chem.* **2002**, *520*, 64–70. [[CrossRef](#)]
48. Lović, J.; Tripković, A.; Gojković, S.L.; Popović, K.D.; Tripković, D.; Olszewski, P.; Kowal, A. Kinetic study of formic acid oxidation on carbon-supported platinum electrocatalyst. *J. Electroanal. Chem.* **2005**, *581*, 294–302. [[CrossRef](#)]

